Microstructural stability of Fe-Cr-Al alloys at 450-550 °C

Jesper Ejenstam[1], Mattias Thuvander[2], Pär Olsson[3], Fernando Rave[4] & Peter Szakalos[1]

[1]KTH Royal Institute of Technology, Division of Surface & Corrosion Science, Drottning Kristinas väg 51, 100 44 Stockholm, Sweden
[2]Chalmers University of Technology, Department of Applied Physics, 412 96 Göteborg, Sweden
[3]KTH Royal Institute of Technology, Division of Reactor Physics, Roslagstullsbacken 21, 106 91 Stockholm, Sweden
[4]Sandvik Heating Technology AB, Box 502, 734 27 Hallstahammar, Sweden

Corresponding author: J. Ejenstam, +46 8 790 6642, ejenstam@kth.se

Abstract

Iron-Chromium-Aluminium (Fe-Cr-Al) alloys have been widely investigated as candidate materials for various nuclear applications. Albeit the excellent corrosion resistance, conventional Fe-Cr-Al alloys suffer from α-α' phase separation and embrittlement when subjected to temperatures up to 500 °C, due to their high Cr-content. Low-Cr Fe-Cr-Al alloys are anticipated to be embrittlement resistant and provide adequate oxidation properties, yet long-term aging experiments and simulations are lacking in literature. In this study, Fe-10Cr-XAl (X=4, 6 and 8) alloys and a Fe-21Cr-5Al were thermally aged in the temperature interval of 450-550 °C for times up to 10,000 h, and the microstructures were evaluated mainly using atom probe tomography. In addition, a kinetic Monte Carlo (KMC) model of the Fe-Cr-Al system was developed. No phase separation was observed in the Fe-10Cr-XAl alloys, and the developed KMC model yielded results in good agreement with the experimental data.

Keywords: Fe-Cr-Al, Thermal Aging, Phase separation, Atom Probe Tomography, kinetic Monte Carlo

1. Introduction

Fe-Cr-Al alloys have lately been proposed as candidate materials for use in various reactor systems, such as the lead cooled fast reactor (LFR) and light water rectors (LWR), due to the ability to form thin, slow growing and corrosion resistant alumina layers on their surfaces [1-9]. Historically, the same alloys have mainly been used as resistance heating elements at temperatures up to about 1300 °C [10]. The composition is typically around 20 wt. % Cr and 5 wt. % Al, with a base of Fe. Because of the high Cr-content, the alloys are not suitable for use at temperatures around 500 °C as the microstructure decomposes into a Fe-rich (α) phase and a Cr-rich (α') phase due to the miscibility gap in the Fe-Cr system [11-16]. This type of phase separation is commonly known as *475 °C embrittlement* or *α-α' phase separation*. As a result of the embrittlement, such alloys are impracticable for use as structural components. The aforementioned power systems all need alloys that can operate in the temperature interval between 300 °C and 700 °C (or higher). However, due to the phase separation issue, conventional Fe-Cr-Al alloys are not realistic alternatives. By lowering the Cr-content of the alloy, the phase separation issue could theoretically be avoided as the phenomenon is governed by the total Cr-content in the ferritic matrix. In literature, phase separation in Fe-Cr-Al has been experimentally studied for a wide range of compositions. During the 1960's, Fe-Cr-Al alloys were extensively studied for use in nuclear applications. Based on hardness measurements, it was proposed that the Cr limit to avoid α-α' phase separation was somewhere in the interval of 10 to 15 wt. %, for a Fe-Cr-4Al alloy [17]. In a more recent study, Kobayashi et al. [18] studied various Fe-Cr-Al alloys, aged at 475 °C for 1000 h. The study resulted in a ternary phase diagram, indicating compositional limits for α-α' phase separation. In addition, the studies showed that the critical Cr-content is shifted towards higher concentrations when Al is added to the system. Recent theoretical studies of the Fe-Cr system have proposed that the Cr solubility in the α phase is more or less constant, around 8 wt. %, at temperatures below 600 K (327 °C), rather than decreasing to about 0 at. % at 300 K (27 °C) [19-21]. Moreover, the calculations have lately been confirmed by thermal aging and irradiation assisted aging experiments [22-25]. The findings show that there is a need to further investigate the long-term effect of Al on the suppression of α-α' phase separation in Fe-Cr-Al alloys with Cr contents higher than 8 wt.%.

This study is part of a larger project aiming at developing corrosion and embrittlement resistant Fe-Cr-Al alloys for use in liquid lead applications, such as LFR. In a previous study by Ejenstam et al. [9] a series of Fe-10Cr-Al alloys showed surprisingly good corrosion resistance when subjected to liquid lead at 550 °C for 10,000 h.

The aim of the work presented here is to thoroughly investigate the long-term microstructural stability of the same alloys from a macroscopic to a microscopic level, by means on thermal aging experiments and kinetic Monte Carlo (KMC) simulations. A conventional Fe-21Cr-5Al alloy is used as a reference material. Moreover, composition limits for avoiding α-α' phase separation, based on simulations, will be presented.

2. Experimental procedures

2.1 Materials and sample preparation

The experimental alloys, produced in collaboration with Sandvik Heating Technology AB, were made in a vacuum induction melting furnace. Roughly 1 kg of each alloy was produced. The ingots were cut into 20×70 mm rods, that were hot-rolled at 1100 °C into wires, in 5 steps, with a final diameter of 4 mm. A 5 minutes heat treatment at 1100 °C was carried out after each hot-rolling step. The analyzed chemical composition of the alloys studied is presented in Table 1.

Thermal aging samples were fabricated from the 4 mm diameter wires, which were further hot-rolled into 8×1 mm strips in 3 steps. Heat treatment at 1100 °C was again carried out between each step. In order to obtain a normalized microstructure, a final 5 min heat treatment at 1100 °C was carried out subsequent to the hot-rolling. Samples for electrical resistance measurement were made from wires, 0.7 mm in diameter, which were produced by reduction of the 4 mm diameter wires by means of dry drawing (5 steps) followed by wet drawing (10 steps).

Table 1. Analyzed chemical compositions of the studied alloys (wt. %).

Alloy	Fe	Cr	Al	Si	C	Ti	Zr
10Cr-4Al	Bal.	10.00	4.03	0.10	0.03	0.08	0.08
10Cr-6Al	Bal.	10.06	6.08	0.03	0.03	0.07	0.08
10Cr-8Al	Bal.	10.09	7.65	0.04	0.03	0.07	0.08
21Cr-5Al	Bal.	21.05	5.04	0.07	0.03	0.08	0.08

Impurity levels: O<0.0035, N<0.003 & S<0.005

2.2 Heat treatment, hardness testing and resistivity measurements

Thermal aging was carried out at 450 °C, 500 °C, and 550 °C in ambient air, and subsequently the samples were air-cooled. Temperatures were controlled using thermocouples (type K), and kept within ±5 °C.

Prior to hardness testing, the samples were molded into bakelite and polished. Fine polishing was carried out in several steps and finalized with an OP-U (chemical polishing solution containing colloidal silica, product of Struers) step. Hardness measurements were carried out using a Mitutoyo MKV-H1 micro-Vickers hardness tester. Indentations were made at four different places on each sample with a force of 5.0 N.

Electrical resistance samples were constructed from 400 mm long Ø0.7 mm wires, which were spiraled. A multimeter (Keithley 2010 low-noise) was connected to each end of the samples, and the resistance was recorded using a data acquisition system controlled by a LabVIEW software. The spiraled samples were heated in a Fibrothal lab furnace, and the temperature, measured using a thermocouple (type K) running through the spiraled samples, was kept within ±5 °C..

2.3 Atom Probe Tomography (APT)

Atom Probe Tomography analyses were carried out using a LEAP 3000X HR from Imago Scientific Instruments. Both voltage and laser pulse modes were used at tip temperatures of 70 K and 50 K, respectively. A frequency of 200 kHz was used for both laser and voltage pulsing. The voltage pulse fraction was 20 %, and the laser pulse energy was 0.3 nJ. The evaporation rate (ions detected per pulse) for both modes was about 1 %. The reason for using laser pulsing, although it can give rise to artifacts [26], was that sample fracture often occurred when analyzing some of the materials. Reference samples displaying phase separation were analyzed by means of both voltage and laser pulse modes with essentially identical results, thus providing credibility for using laser pulsing. It should be noted that the laser pulse energy used here (0.3 nJ) was much lower than in [26] (0.6-2.0 nJ). Needle shaped specimens were prepared using the standard two-step electrochemical polishing method, and the acquired data were analyzed using the IVAS 3.4.3 software. In order to extract information about phase separation, the APT data sets were evaluated using concentration frequency diagrams (with a block size of 50 ions) and radial distribution functions (RDF). It was found that the latter method was more sensitive and therefore only results from this method are presented below. The advantages of using RDFs are further discussed in [27].

Before constructing RDFs, the regions in proximity of major crystallographic poles were removed, as the measured Cr concentration in these regions is erroneously high (because of preferential evaporation of Fe). As there is an overlap in the mass spectrum at mass-to-charge state ratio 27 Da (or more precisely at 26.97 Da) between the minor isotopes ^{54}Cr and ^{54}Fe, this peak was assigned neither to Cr, nor to Fe. In the analyses obtained using laser pulsing, giving a lower evaporation field, the peak at 27 Da was assigned to Al. Moreover, only analyses containing at least 3 million atoms were included in the evaluation.

2.4 Scanning Electron Microscopy (SEM)

Fracture surface analysis, of samples fractured in a bending test, was carried out using a Hitachi TM-1000 tabletop scanning electron microscope. Images were captured at an acceleration voltage of 10 kV using a backscattered electron detector.

3. Atomistic modeling of aging

The evolution of an alloy system can be modeled using stochastic methods, such as the KMC algorithm. The underlying vibrations and dynamics are replaced by state-to-state transitions, and thus an aging kinetic can be well represented considering that the dominating atomic diffusion mechanism is vacancy mediated.

KMC simulations were performed with the LAKIMOCA code [28]. Diffusion occurs via vacancy jumps towards nearest neighbor (nn) atoms. For Fe-Cr-Al alloys, the underlying lattice is body centered cubic (bcc) for all Fe-rich compositions. The simulated crystal is thus constructed on a rigid bcc lattice with periodic boundary conditions. In order to drive the aging process, a single vacancy is introduced in the simulation box. The aging kinetics is simulated in boxes with sizes (S) equal to $32a_0$ (65 536 sites) and $100a_0$ (2 048 000 sites) with a_0 = 0.28553 nm. Results are averaged over 20 simulations for S = $32a_0$ and over 5 simulations in the case of S = $100a_0$. The residence time algorithm [29] is employed to ascribe a time step to each event. In the bcc lattice, under thermal conditions, there are eight possible transitions corresponding to the eight first nearest neighbor vacancy jumps. The jump frequencies, Γ_x, are given by:

$$\Gamma_x = \nu \, exp\left(-\frac{E^x_{mig}+{\Delta E}/{2}}{k_b T}\right), \qquad (1)$$

where x defines the jumping atom and ν the attempt frequency (6×10^{12} s^{-1}). The migration energies, E^x_{mig}, are here calculated *ab initio* in the framework of density functional theory (DFT) with the Vienna Ab initio Simulation Package (VASP) [30-32]. The projector augmented wave formalism [33, 34] was employed with the standard Perdew-Burke-Ernzerhof pseudopotentials [35] for Fe, Cr and Al. Periodic boundary conditions were applied on cubic constant volume supercells of 128 bcc sites, where only the internal degrees of freedom were relaxed, using the conjugate gradient algorithm. The Brillouin zone sampling was performed with 27 k points using the Monkhorst and Pack scheme [36]. The equilibrium lattice parameter for bcc Fe was used for all supercell calculations and the plane wave cutoff energy was 300 eV. The convergence of the binding energies with these parameters is about 10 meV [37]. The migration barriers thus calculated are 0.71 eV for Fe, 0.54 eV for Cr and 0.48 eV for Al for the vacancy mechanism. The energy difference between the initial and final states, ΔE, was calculated using an interatomic potential. The cohesive model used to determine the system energy is based on the two-band model (2BM) [38] for Fe-Cr alloys, with the addition of rigid lattice potentials (RLP) for the Al-Fe, Al-Cr and Al-Al interactions. This RLP uses the density and embedding energy of Fe from the 2BM [39] while new pair potential contributions are given here in Table 2, where also the DFT predictions, on which the RLP is based, are given. The sign convention for the binding

energies is such that positive values imply attraction. The pair potential parameters were fitted to reproduce exactly the DFT predictions for the solute–solute and solute–vacancy interactions up to the cut-off after the third nearest neighbor.

Table 2. Fitting parameters for the Al-Al, Al-Fe and Al-Cr rigid lattice pair potentials.

DFT configuration	E_b (Al-Al) (eV)	E_b (Al-vac) (eV)	E_b (Al-Cr) (eV)
1nn	–0.1367	0.3183	–0.0631
2nn	–0.1133	–0.0339	–0.0882
3nn	0.0035	0.0204	–0.0062
RLP separation distance (nm)	V (Al-Al) (eV)	V (Al-Fe) (eV)	V (Al-Cr) (eV)
0.24727 [1nn]	0.5274	0.3908	0.3002
0.28553 [2nn]	–0.2103	–0.1329	–0.1639
0.40380 [3nn]	0.0009	–0.0086	–0.0077

The physical time attached to the Monte Carlo step is the average time step, defined as $\tau = 1/\Sigma\Gamma_x$. However, the vacancy concentration is normally much higher in the simulation cell than in experimental conditions, and thus the simulation time has to be rescaled. The physical time is related to the Monte Carlo time by a factor $S_v = C_v/C_v^{eq}(T)$ where C_v is the vacancy concentration in the simulated system and $C_v^{eq}(T)$ is the thermal equilibrium concentration. For low solute concentrations, $C_v^{eq}(T)$ can be computed using the vacancy formation energy in the pure solvent metal. When the solute concentration is high, the vacancy formation energy is likely to be different. In a previous study of spinodal decomposition in Fe-Cr alloys, direct comparison between simulation and APT experiments showed that the equilibrium vacancy concentration is well described by evaluating the Boltzmann factor $C_v^{eq}(T) = \exp\left(-\frac{G_f}{k_B T}\right)$ with the theroretical average vacancy formation energy for the given alloy composition [40]. Here, the same procedure was applied. The KMC simulations were performed in the rigid lattice approximation, thus neglecting the contribution of vibrational entropy, in similar vein as in a large number of studies of the binary Fe-Cr system [20, 38, 40-42]. For the 2BM, this leads to a shift of the solubility line at 500 °C of –2.5 at. %. Consequently, for the composition here denoted Fe-10Cr-Al, a Cr concentration of 7.5 at. % will be used in the simulation.

In order to assess phase stability as a function of composition, Metropolis Monte Carlo (MMC) simulations [43] can be performed. In this algorithm, the system is driven towards its thermodynamic equilibrium much more efficiently than in the KMC algorithm, although not through the physically correct mechanism. It is, however, convenient to use MMC to estimate phase boundaries, since it samples the configurational entropy and the enthalpies, neglecting only the vibrational entropy contribution.

4. Results

4.1 Micro-Vickers hardness and bending test

The results from the Vickers hardness testing show a clear hardening of the reference alloy, 21Cr-5Al, after aging at 450 °C and 500 °C, whereas no significant hardening is observed for the 10Cr-alloys, Fig. 1. The hardness increase in the reference alloys is measurable already after 10 hours of aging at both temperatures, and it seems to level off after 1000 hours. Some hardening is noted for the 10Cr-alloys as well, although not as significant as for the reference alloy. None of the alloys showed any significant hardening subsequent to aging up to 10,000 hours at 550 °C. Furthermore, an increase in average hardness with increased Al content was observed for the 10Cr-alloys.

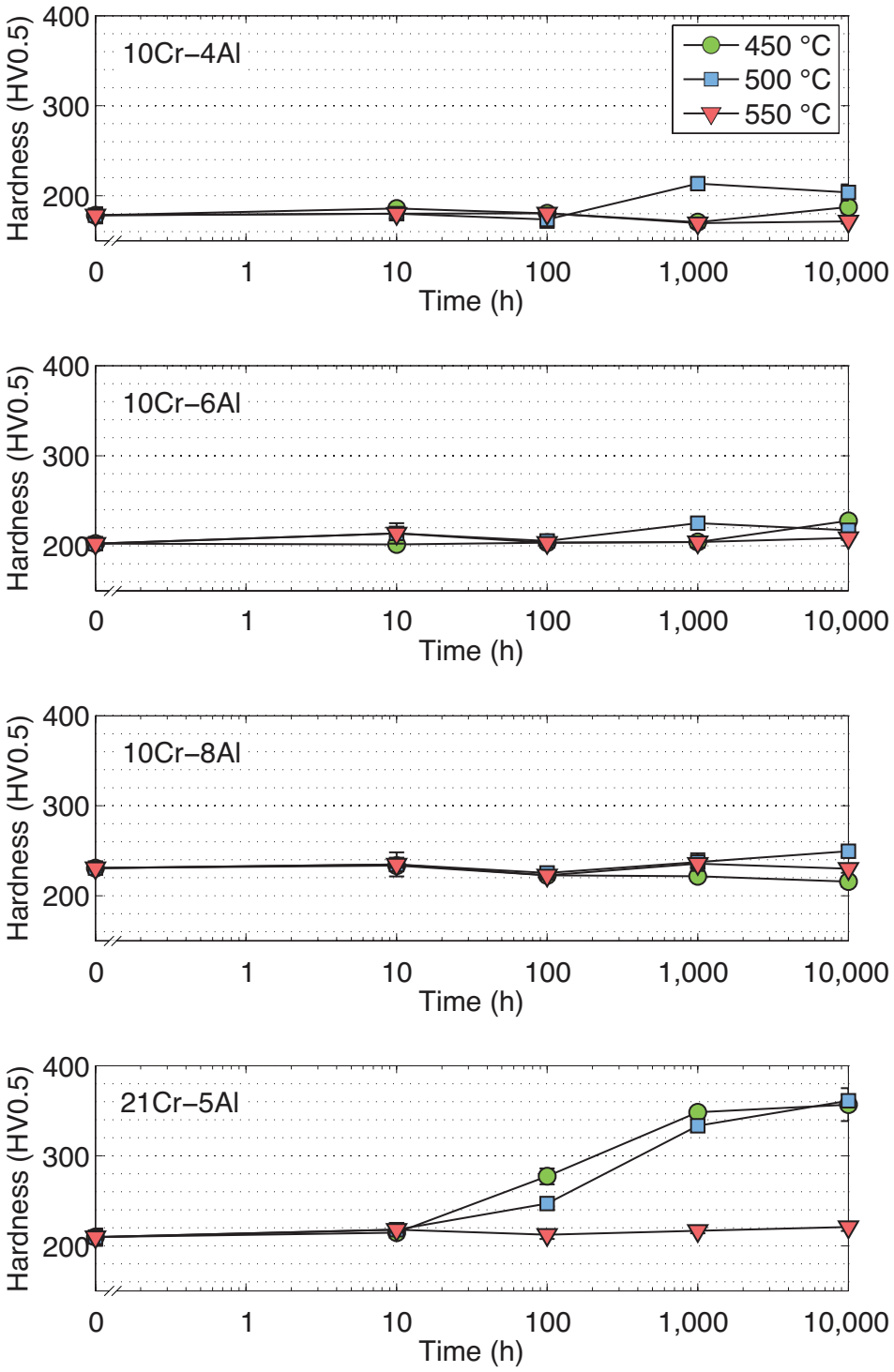

Fig. 1. Vickers hardness as a function of aging time for all experimental alloys. A fast increase in hardness is seen for the 21Cr-5Al alloy aged at 450 °C and 500 °C, but not at 550 °C. The 10Cr-alloys show no significant hardness change at any of the temperatures.. Note that the error bars, indicating the standard deviation of the measurements, are small and for most data points covered by the markers.

In addition to hardness testing, a bending test was carried out at room temperature for the samples aged for 10,000 h, in which they were manually bent to an angle >90° in order to qualitatively evaluate brittleness. The samples were clamped in a vise, with copper strips in-between the sample and the tool, and bent. All 10Cr-alloys were bent to angles >90° without any crack initiation. For the reference alloy, however, only the 550 °C-sample could be bent to an angle >90°. The samples aged at 450 °C

and 500 °C suffered from brittle fractures, at angles about 20-30°, when force was applied, Table 3 and Fig. 2.

Table 3. Results from the bending test of samples aged for 10,000 h. The reference alloy samples suffered from brittle fractures when aged at 450 °C and 500 °C. All other samples were successfully bent to angles >90°.

Alloy	450 °C	500 °C	550 °C
10Cr-4Al	No fracture	No fracture	No fracture
10Cr-6Al	No fracture	No fracture	No fracture
10Cr-8Al	No fracture	No fracture	No fracture
21Cr-5Al	Brittle fracture (20-30°)	Brittle fracture (20-30°)	No fracture

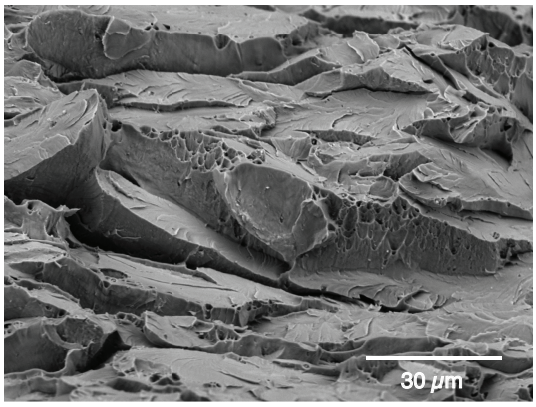

Fig. 2. Backscattered electron SEM micrograph of the bend-test fracture surface of 21Cr-5Al, aged at 500 °C for 10,000 h. The fracture surface displays a typical brittle morphology.

4.2 Electrical resistance measurement

Electrical resistance measurements were carried out *in-situ* on the reference alloy, 21Cr-5Al, and the 10Cr-4Al-alloy, during aging for 48 h at the temperatures 450, 475, 500 and 550 °C. This method is highly sensitive to changes in the microstructure. Hence, phase separation processes can be detected in real time. The relative change in electrical resistance between unaged samples and the samples aged for 48 h is presented in Fig. 3. The reference alloy shows a significant decrease in resistance for the three temperatures 450, 475 and 500 °C, with the largest decrease occurring at 475 °C, i.e. at the temperature where the α-α' phase separation is known to be as fastest. Also the 10Cr-4Al alloy shows a decrease in resistance for these temperatures, but the decreases are very small (and do not follow the pattern with a maximum decrease at an intermediate temperature). Aging at 550 °C resulted in a minute increase in resistance for both alloys.

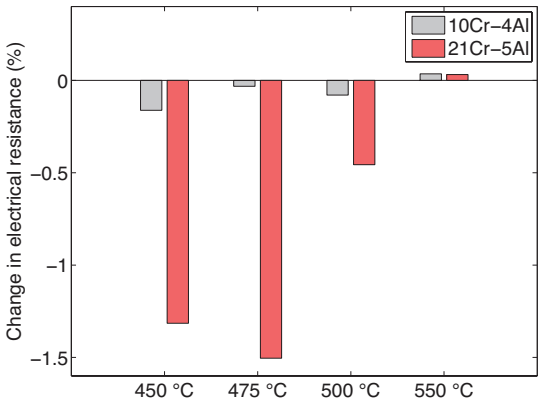

Fig. 3. Change in electrical resistance following aging for 48 h at 450 °C, 475 °C, 500 °C and 550 °C for 10Cr-4Al and 21Cr-5Al.

4.3 Atom Probe Tomography

Three alloys, 10Cr-4Al, 10Cr-8Al and 21Cr-5Al, were studied by means of APT in order to evaluate the homogeneity of the microstructure on the atomic scale. The two 10Cr-alloys were aged at 500 °C for 10,000 h, whereas the 21Cr-5Al alloy was aged for only 48 h at 475 °C and 500 °C, *i.e.* the electrical resistance samples were used in the case of 21Cr-5Al. The reason for choosing these samples for APT was that electrical resistance measurements had clearly indicated phase separation in 21Cr-5Al already after 48 h, whereas phase separation in the 10-Cr alloys, if at all possible, must be very slow. The APT analyses did not show any sign of inhomogeneities in any of the aged 10Cr-alloys, Fig. 4b and 4c. In addition, no distinguishable differences are noted when comparing with an unaged 10Cr-4Al sample, Fig. 4a. Clustering of Cr atoms was apparent in the atom maps of the 21Cr-5Al alloy when aged at 500 °C and 475 °C, Fig. 4d and 4e.

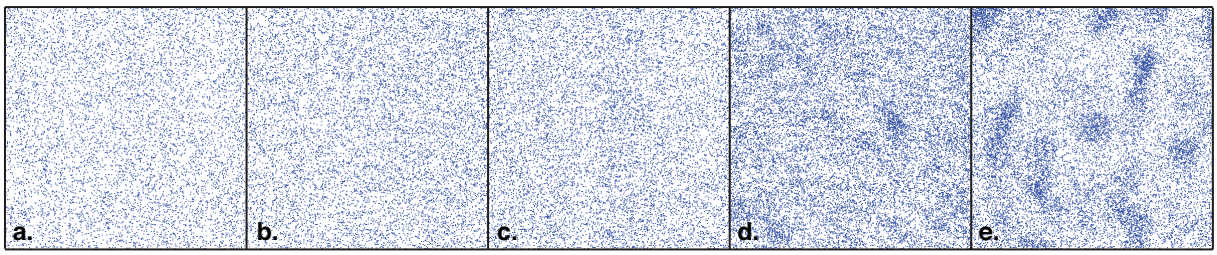

Fig. 4. Maps showing the distribution of Cr atoms in a 30×30×3 nm slice of aged and unaged material. (a.) 10Cr-4Al, unaged, (b.) 10Cr-4Al, 10,000 h at 500 °C, (c.) 10Cr-8Al,10,000 h at 500 °C, (d.) 21Cr-5Al, 48 h at 500 °C, (e.) 21Cr-5Al, 48 h at 475 °C.

Moreover, the tendency of Cr clustering is clearly higher when the reference alloy is aged at the lower temperature. The morphology and the rough size of the clusters are clearly seen in Fig. 5, which shows iso-concentration surfaces made using a threshold of 27 wt. % Cr. In RDF plots, a strong positive interaction between Cr atoms is evident in the reference alloy, whereas no or little interaction is seen for the 10Cr-alloys, Fig. 6a. The RDFs show the average Cr concentration as function of the radial distance from other Cr atoms in the volume. The calculation is carried out for all Cr atoms in the volume, and the concentration is normalized with the average Cr concentration in the volume and summed up. In a homogenous material, the RDF value is therefore equal to unity for all distances. Analyzing an unaged sample of the 10Cr-4Al alloy also shows a small positive interaction of Cr atoms at very short distances (<1 nm), thus the small positive interaction in the aged 10Cr-samples is not likely caused by α-α' phase separation during aging. Apart from Cr clustering in the reference alloy, no other phase separation or precipitation was noted in the APT analysis. In case of the Al distribution in the aged 21Cr-5Al sample, it was found that Al had a weak preference for the Fe rich α phase, Fig. 7.

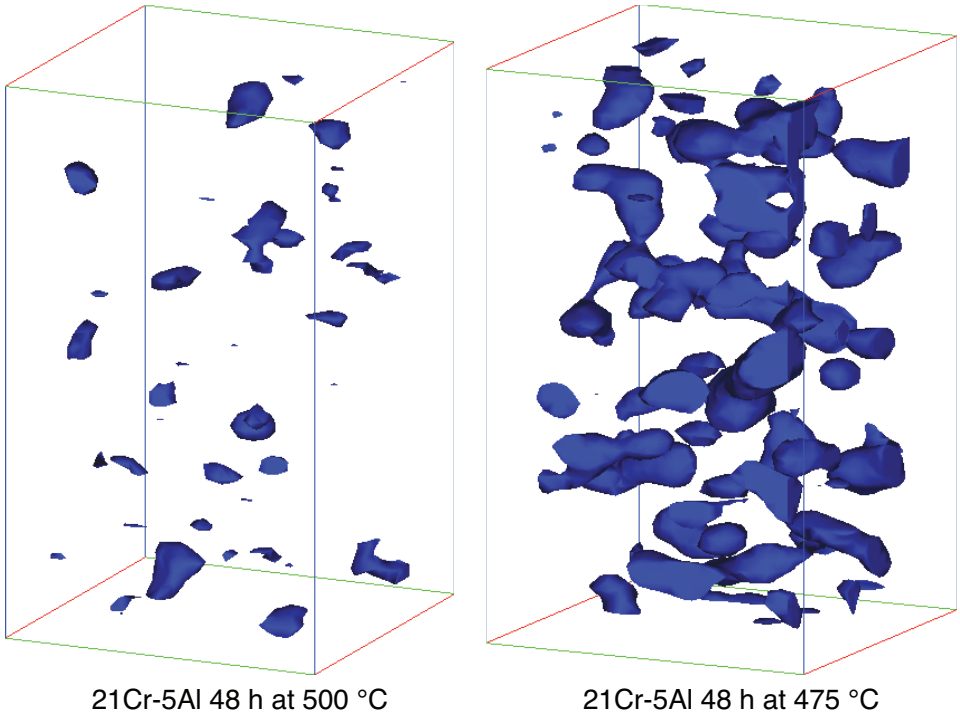

Fig. 5. Volumes (30×30×50 nm) showing 27 wt. % Cr iso-concentration surfaces for the reference sample aged 48 h at 500 °C and 48 h at 475 °C, respectively.

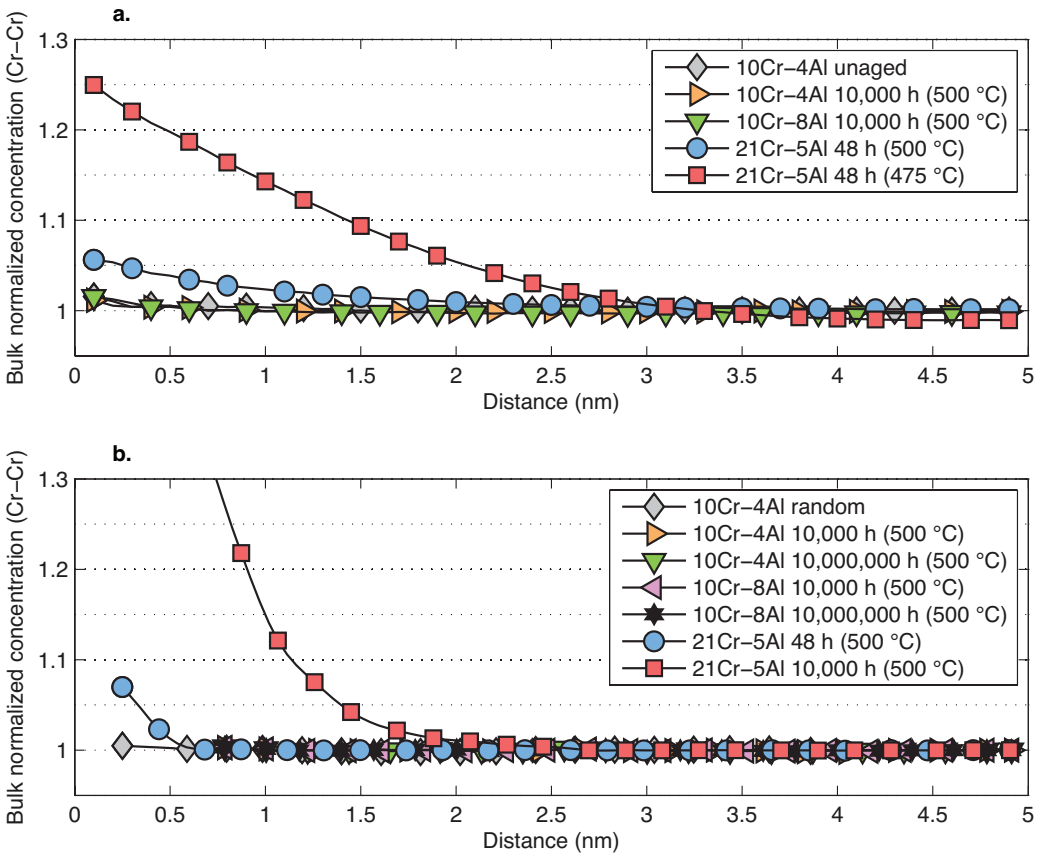

Fig. 6. (a.) Curves showing RDFs for Cr-Cr in aged and unaged material. (b.) Simulated RDFs from the 10Cr-alloys and 21Cr-5Al, aged for different times at 500 °C. A random distribution 10Cr-4Al is simulating unaged material.

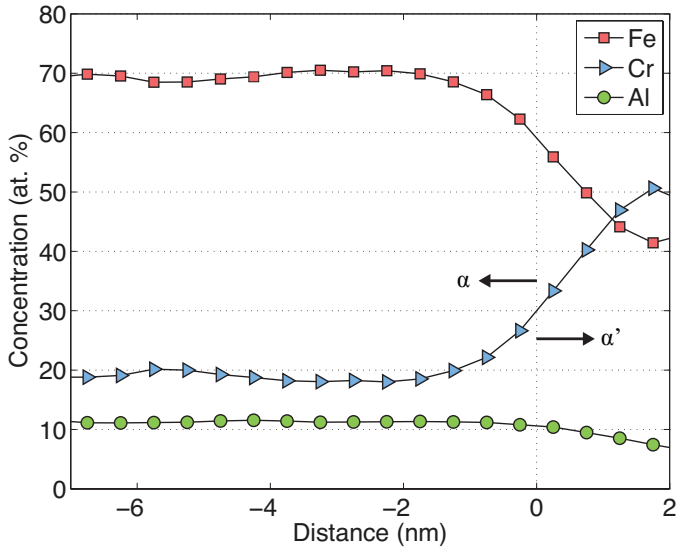

Fig. 7. Proximity histogram of the analyzed reference sample (27 wt. % iso-concentration surfaces), aged at 475 °C for 48 h, showing a slight decrease in Al concentration within the Cr rich α' phase.

4.4 Simulated aging and phase stability

KMC simulations were performed at 500 °C for the compositions 10Cr-4Al, 10Cr-8Al and 21Cr-5Al. For the 10Cr-alloys, the bulk normalized radial Cr-Cr distribution functions stay very close to unity for distances larger than 0.7 nm, in good agreement with the measured RDF using APT, Fig. 6b. In addition, the composition of the (48 h) simulated α' phase implied an enrichment of Cr to about 50 at. %, which is in good agreement with the measurement presented in Fig. 7. Aluminium was observed to have a distinct preference for the α phase in the simulation, as it decreased to about 2.5 at. % in the precipitates. The simulated Cr-Cr RDFs of the 10Cr-alloys are, however, not shown for the first coordination shells. The strong Cr-Cr repulsion, predicted for dilute Cr in Fe from DFT [44, 45], causes local domain ordering [45] and a consequent dip in the short range RDF that reduces the resolution for the longer distances. The simulations on the 10Cr-alloys were continued for up to 10,000,000 h of simulated time without showing any sign of α-α' phase decomposition. For the 21Cr-5Al alloy the phase decomposition is evident, as in the measurements, after only 48 h.

The Al solutes are, in all conditions here considered, partitioning preferentially to the α phase, in agreement with experiments in this study and in literature [16]. The Cr solubility in Fe-Cr-Al alloys has recently been estimated through hardness measurements [18]**.** There the solubility limit was estimated by tracing the compositions for which the hardness increase was ≥50 H_V after 1000 h of aging at 475 °C. Here, the results from MMC simulations are compared with that estimate and a qualitative agreement is noted, Fig. 8. The dashed lines in Fig. 8 show the actual MMC results, while the solid lines display the prediction including the correction in Cr content, as described above. The slight curvature indicating larger Cr solubility with increasing Al content, after a threshold of about 5 at. % Al, is well reproduced by the model.

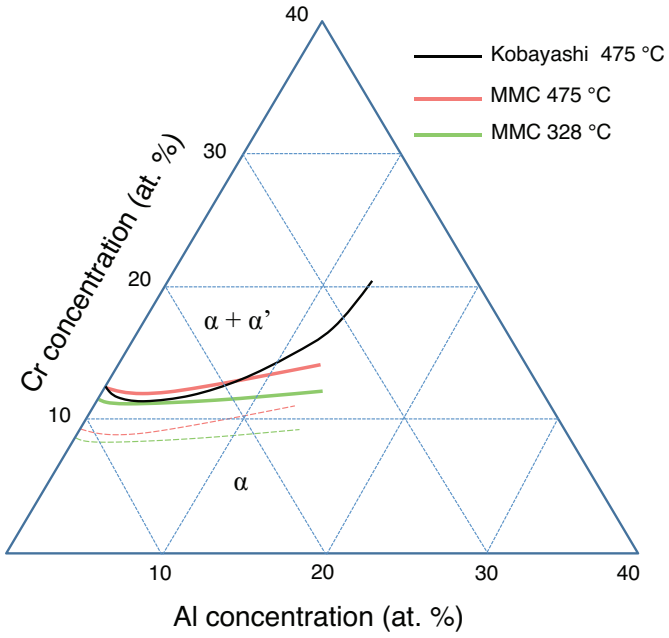

Fig. 8. The solubility limits as estimated by experiments [18] and using MMC simulations, for 328 °C and 475 °C. The dashed lines comes directly from the model and the solid lines are corrected predictions.

5. Discussion

After aging up to 10,000 hours, the samples were evaluated by means of micro-Vickers hardness testing. This evaluation shows a clear hardening effect in the 21Cr-5Al reference material after some tens of hours, which is expected due to the high Cr content. This is a well-known effect that has been extensively studied in literature both for Al and non-Al bearing Fe-Cr alloys [11-16]. The main purpose of this paper is to experimentally show that the Fe-10Cr-Al alloys do not suffer from any microstructural degradation related to the miscibility gap in the Fe-Cr phase diagram. The hardness test showed no significant increase in hardness for any of the 10Cr-alloys. However, small changes were noted after long times. These changes are likely derived from precipitates, such as carbides and nitrides. The increased bulk hardness with increasing Al content, is a typical behavior of solid solution hardening, which causes higher tension in the crystal structure. A qualitative bending test was conducted for all alloys aged up to 10,000 hours, which indicated that the 10Cr-alloys preserved their ductility. The reference alloy, however, did suffer brittle fracture when a bending force was applied.

Short-term aging for up to 48 h was conducted, during which the change in electrical resistance was continuously measured. In 1957, Williams et al. [11] used this method in one of the first studies that showed the presence of a miscibility gap in the Fe-Cr system. The α-α’ phase separation results in a modulation of the material's composition [46]. This means that pathways, which are better electrical conductors, are formed due to change in local composition, thus the electrical resistance is reduced while the material is aged in the critical temperature interval [47]. As for the hardness test, the reference alloy showed clear signs of phase separation, indicated by a decrease in the electrical resistance during short-term aging. α-α’ phase separation is often related to as 475 °C embrittlement as the kinetics is the fastest around this temperature, which also was evident in the electrical resistance measurement. The largest decrease in electrical resistance was noted at 475 °C, slightly larger than at 450 °C. At 500 °C the decrease was only about one third as large as at 475 °C. For the 10Cr-4Al alloy, minor changes in electrical resistance were noted, however, these changes are likely to stem from precipitation of carbides and/or nitrides, and not from α-α’ phase separation. The non-systematic change in electrical resistance over the temperature interval, as well as observations in literature [13], supports this conclusion.

In order to investigate the microstructure in detail on the atomic scale, APT analyses were conducted. The analyses showed fully homogeneous microstructures for the two investigated 10Cr-alloys, 10Cr-4Al and 10Cr-8Al, aged for 10,000 h at 500 °C. No enrichment of any alloying elements was found in any of the analyzed samples. The analyzed volumes of the reference 21Cr-5Al alloy, aged for 48 h at 475 °C and 500 °C, showed clear signs of Cr clustering. In addition, a slight partitioning effect towards the α phase was noted for Al. These samples were analyzed in order to quantify the size and density of phase separation and to directly couple these to the reduction in electrical resistivity. The results show that this may be done qualitatively, however, more work has to be carried out to allow the microstructure to be quantitatively described from the electrical resistance measurements alone. Radial distribution function analysis has in previous studies been shown to be a powerful tool to study phase separation in a material [27]. By calculating the RDF clustering can be statistically shown. Furthermore, the size and periodicity of such clusters can be determined using this method. As for the volume analyses of the 10Cr-alloys, calculated RDFs showed fully homogeneous microstructures, whereas for the reference 21Cr-5Al alloy clear Cr clustering was observed. For the first few coordination shells, that is for short distances smaller than 0.5 nm, a small increase is seen for the 10Cr-alloys, both in unaged and aged materials. Similar behavior has previously been noted in literature for Fe-20Cr alloys [48], however, the cause is unclear. The increased clustering of Cr atoms

in the reference alloy at 475 °C and 500 °C are in line with the other measurements and the fact that the kinetics is faster at 475 °C.

The thermal aging simulations are validated in comparison to the experimental results and provide also an extrapolation in time, showing that the 10Cr-alloys should remain indefinitely in the α phase at these temperatures. In the simulation, the characteristic size of the precipitates is, however, much smaller than in the experiment, an effect that has been noted before in binary Fe-Cr alloys, even though the evolution of the characteristic size was in good agreement with experiments [40]. Moreover, the simulated composition of the α' phase was close to the measured value presented in Fig. 7. When continuing the simulations up to one year of simulation time, the size is seen to have grown far beyond the 0.7 nm separation distance. Therefore, if the 10Cr-alloys were to decompose, it would have been clearly visible even when excluding the short range RDF.

Moreover, the predicted effect of Al addition on the Cr solubility, which ultimately affects the 475 °C embrittlement, is in qualitative agreement with previous experiments, albeit with a shift in Cr content, described above. Assuming that the temperature trend in the simulation is correct and that the Cr content shift is the main error, the simulations allow predicting the solubility as a function of temperature. The reason for the increased solubility in the model is an effective screening of the Cr-Cr interactions in the Fe matrix by the Al solutes. In a recent theoretical study, similar predictions of the solubility limits were obtained based on *ab initio* calculations of bulk and interface properties of Fe-Cr-Al alloys [49]. Furthermore, in Fig. 8 a slight weakening of the Al effect on the Cr solubility with decreasing temperature is noted. The simulated solubility line at 328 °C (melting point of lead) has a smaller curvature than at 475 °C and thus the beneficial effect of Al addition on phase decomposition is here predicted to be slightly smaller at lower temperatures.

Adding Al to the Fe-Cr alloy system is not exclusively beneficial. Aluminium has been shown to be detrimental to strength [50] and to impair the weldability of the alloy [51]. Thus, it is crucial to find the optimal composition of the alloy, so that it still possesses good corrosion resistance, resistance to α-α' phase separation, and has adequate weldability and strength properties. Commercial Fe-Cr-Al alloys are limited to about 5-6 wt.% Al, and yet welding is difficult. Therefore, optimizing embrittlement resistant Fe-Cr-Al alloys at lower Al (and Cr) concentrations, with maintained oxidation properties, is proposed for nuclear applications. The limit composition to avoid α-α' phase separation for a suggested 4Al-alloy at 475 °C is here predicted to be 13Cr-4Al, while at 328 °C it would be closer to 11Cr-4Al. Consequently, for safe operation of such a material in an LFR, the Cr content should be limited accordingly. The 10Cr-4Al alloy is thus the most promising alloy candidate in the 10Cr-alloy series. For an eventual deployment in a reactor environment, further studies of the radiation tolerance of these materials are necessary, and the here developed simulation model can be extended for studying, for example, irradiation effects due to point defect diffusion and clustering.

Conclusions

In this study, Fe-10Cr-Al alloys and a Fe-21Cr-5Al reference alloy were thermally aged in the temperature interval of 450 °C to 550 °C up to 10,000 h in order to study the alloys' microstructural stability. In parallel, a KMC model of the Fe-Cr system was expanded with Al, and the results of both experimental work and simulations were compared.

- No signs of microstructural degradation related to α-α' phase separation were seen in any of the Fe-10Cr-Al alloys in this study. APT analyses of material aged up to 10,000 h showed fully homogenous microstructures.
- The reference Fe-21Cr-5Al alloy was readily embrittled in the interval of 450-500 °C, and presented results are in good agreement with reports in literature.
- KMC simulations, based on the two-band model for Fe-Cr alloys extended with Al interactions, yielded results in agreement with experiments.
- A long-term (10,000,000 h) KMC thermal aging simulation of the Fe-10Cr-Al system was carried out at 500 °C, in which no α-α' phase separation occurred.
- Simulated composition limits to avoid α-α' phase separation were calculated to 13Cr-4Al at 475 °C and 11Cr-4Al at 328 °C.

6. Acknowledgements

The authors are grateful to Sandvik Heating Technology AB for the production of the experimental alloys and the overall support of the project. Special thanks to B. Jönsson, D. Chandrasekaran, P. Byhlin, F. Jämtefors and J. Nockert Olovsjö. Thanks also to Prof. I. Odnevall Wallinder, Division of Surface and Corrosion Science, KTH and Prof. J. Wallenius, Division of Reactor Physics, KTH for guidance. The high performance computing resources were provided by the Swedish National Infrastructure for Computing (SNIC) centers PDC (Lindgren) and NSC (Triolith) and by the Swiss CSC resource ROSA through the PRACE-2IP project (FP7 RI-283493). Last, but not least, the authors would like to thank the Göran Gustafsson Stiftelse, the Swedish Research Council (VR) and the GENIUS project for funding and support.

7. References

[1] G. Muller, G. Schumacher, F. Zimmerman, J. Nucl. Mater., 278 (2000) 85-95.
[2] M. Kondo, M. Takahashi, J. Nucl. Mater., 356 (2006) 203-212.
[3] S. Takaya, T. Furukawa, K. Aoto, G. Muller, A. Weisenburger, A. Heinzel, M. Inoue, T. Okuda, F. Abe, S. Ohnuki, T. Fujisawa, A. Kimura, J. Nucl. Mater., 386 (2009) 507-510.
[4] J. Lim, H.O. Nam, I.S. Hwang, J.H. Kim, J. Nucl. Mater., 407 (2010) 205-210.
[5] M. Del Giacco, A. Weisenburger, A. Jianu, F. Lang, G. Mueller, J. Nucl. Mater., 421 (2012) 39-46.
[6] T. Cheng, J.R. Keiser, M.P. Brady, K.A. Terrani, B.A. Pint, J. Nucl. Mater., 427 (2012) 396-400.
[7] B.A. Pint, K.A. Terrani, M.P. Brady, T. Cheng, J.R. Keiser, J. Nucl. Mater., 440 (2013) 420-427.
[8] A. Weisenburger, A. Jianu, S. Doyle, M. Bruns, R. Fetzer, A. Heinzel, M. DelGiacco, W. An, G. Muller, J. Nucl. Mater., 437 (2013) 282-292.
[9] J. Ejenstam, M. Halvarsson, J. Weidow, B. Jönsson, P. Szakalos, J. Nucl. Mater., 443 (2013) 161-170.
[10] B. Jonsson, R. Berglund, J. Magnusson, P. Henning, M. Hattestrand, High Temperature Corrosion and Protection of Materials 6, Prt 1 and 2, Proceedings, 461-464 (2004) 455-462.
[11] R.O. Williams, H.W. Paxton, J Iron Steel Inst, 185 (1957) 358-374.
[12] R. Lagneborg, Acta Metall Mater, 15 (1967) 1737-1745.
[13] W.S. Spear, D.H. Polonis, Metall Mater Trans A, 25 (1994) 1135-1146.
[14] J.H. Lange, M. Brede, B. Fischer, S. Spindler, H. Wagner, R. Wittmann, D. Gerthsen, A. Broska, J. Wolff, MRS Online Proceedings Library, 539 (1998).

[15] C. Capdevila, M.K. Miller, K.F. Russell, J. Chao, J.L. Gonzalez-Carrasco, Mat Sci Eng a-Struct, 490 (2008) 277-288.
[16] C. Capdevila, M.K. Miller, K.F. Russell, J Mater Sci, 43 (2008) 3889-3893.
[17] J.L. Bartos, The Nature of Aging of Fe-Cr-Al-Y Alloys at 450 C, General Electric Company, Nuclear Systems Programs, 1969, Report No. GEMP 709.
[18] S. Kobayashi, T. Takasugi, Scripta Mater, 63 (2010) 1104-1107.
[19] P. Olsson, I.A. Abrikosov, L. Vitos, J. Wallenius, J. Nucl. Mater., 321 (2003) 84-90.
[20] G. Bonny, D. Terentyev, L. Malerba, Scripta Mater, 59 (2008) 1193-1196.
[21] W. Xiong, M. Selleby, Q. Chen, J. Odqvist, Y. Du, Crit Rev Solid State, 35 (2010) 125-152.
[22] M. Mathon, Y. de Carlan, G. Geoffroy, X. Averty, C.H. de Novion, A. Alamo, Microstructural Evolution of Reduced Activation and Conventional Martensitic Steels after Thermal Aging and Neutron Irradiation, S.T. Rosinski, M.L. Grossbeck, T.R. Allen, A.S. Kumar (Eds.), in: Effects of Radiation on Materials: 20th International Symposium, American Society for Testing and Materials, West Conshohocken, PA, (2001)
[23] M.H. Mathon, Y. de Carlan, G. Geoffroy, X. Averty, A. Alamo, C.H. de Novion, J. Nucl. Mater., 312 (2003) 236-248.
[24] V. Kuksenko, C. Pareige, P. Pareige, J. Nucl. Mater., 432 (2013) 160-165.
[25] M. Bachhav, G.R. Odette, E.A. Marquis, Scripta Mater, 74 (2014) 48-51.
[26] M.D. Mulholland, D.N. Seidman, Microsc Microanal, 17 (2011) 950-962.
[27] J. Zhou, J. Odqvist, M. Thuvander, P. Hedstrom, Microsc Microanal, 19 (2013) 665-675.
[28] C. Domain, C.S. Becquart, J.C. Van Duysen, Kinetic Monte Carlo simulations of cascades in Fe alloys, in: Materials Research Society Symposium - Proceedings, 2001, pp. R3.25.21-R23.25.26.
[29] W.M. Young, E.W. Elcock, Proceedings of the Physical Society, 89 (1966) 735-746.
[30] G. Kresse, J. Hafner, Phys Rev B, 47 (1993) 558-561.
[31] G. Kresse, J. Hafner, J Phys-Condens Mat, 6 (1994) 8245-8257.
[32] G. Kresse, J. Hafner, Phys Rev B, 49 (1994) 14251-14269.
[33] P.E. Blochl, Phys Rev B, 50 (1994) 17953-17979.
[34] G. Kresse, D. Joubert, Phys Rev B, 59 (1999) 1758-1775.
[35] J.P. Perdew, K. Burke, M. Ernzerhof, Phys Rev Lett, 77 (1996) 3865-3868.
[36] H.J. Monkhorst, J.D. Pack, Phys Rev B, 13 (1976) 5188-5192.
[37] P. Olsson, T.P.C. Klaver, C. Domain, Phys Rev B, 81 (2010)
[38] P. Olsson, J. Wallenius, C. Domain, K. Nordlund, L. Malerba, Phys Rev B, 72 (2005)
[39] G.J. Ackland, M.I. Mendelev, D.J. Srolovitz, S. Han, A.V. Barashev, J Phys-Condens Mat, 16 (2004) S2629-S2642.
[40] C. Pareige, M. Roussel, S. Novy, V. Kuksenko, P. Olsson, C. Domain, P. Pareige, Acta Mater, 59 (2011) 2404-2411.
[41] J. Wallenius, P. Olsson, C. Lagerstedt, N. Sandberg, R. Chakarova, V. Pontikis, Phys Rev B, 69 (2004)
[42] G. Bonny, D. Terentyev, L. Malerba, D. Van Neck, Phys Rev B, 79 (2009)
[43] N. Metropolis, A.W. Rosenbluth, M.N. Rosenbluth, A.H. Teller, E. Teller, The Journal of Chemical Physics, 21 (1953) 1087-1092.
[44] P. Olsson, C. Domain, J. Wallenius, Phys Rev B, 75 (2007)
[45] C. Pareige, C. Domain, P. Olsson, J Appl Phys, 106 (2009)
[46] D.T. Spreng, J.E. Hilliard, J.W. Kauffman, J Appl Phys, 43 (1972) 2040-2047.
[47] Y.Y. Tsiovkin, A.N. Voloshinskii, V.V. Gapontsev, V.V. Ustinov, A.G. Obykhov, A.L. Nikolaev, I.A. Nekrasov, A.V. Lukoyanov, Phys Rev B, 72 (2005)
[48] P. Hedström, F. Huyan, J. Zhou, S. Wessman, M. Thuvander, J. Odqvist, Materials Science and Engineering: A, 574 (2013) 123-129.
[49] W. Li, S. Lu, Q.-M. Hu, H. Mao, B. Johansson, L. Vitos, Comp Mater Sci, 74 (2013) 101-106.
[50] A. Kimura, R. Kasada, N. Iwata, H. Kishimoto, C.H. Zhang, J. Isselin, P. Dou, J.H. Lee, N. Muthukumar, T. Okuda, M. Inoue, S. Ukai, S. Ohnuki, T. Fujisawa, T.F. Abe, J. Nucl. Mater., 417 (2011) 176-179.
[51] J.R. Regina, J.N. Dupont, A.R. Marder, Weld J, 86 (2007) 170S-178S.